Modeling damage evolution of the near-fault region as a result of rupture on a geometrically complex fault

Khurram S. Aslam[1]; Eric G. Daub[1]
[1]CERI, University of Memphis, Memphis, USA
Contact: Khurram Aslam (ksaslam@memphis.edu)

Why this study

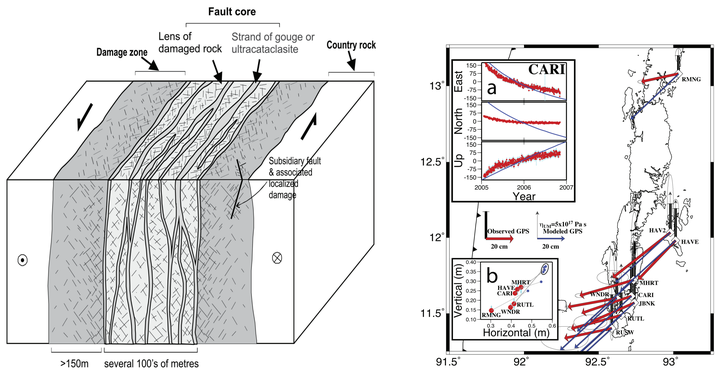

▲ **Figure 1**. (Left) Typical strike-slip fault zone structures in a quartzofeldspathic country rock (reproduced from Faulkner et al., 2003). (Right) GPS observed post-seismic displacements for the Andaman Islands since the 2004 earthquake (Paul et al., 2005).

Motivation

Real faults exhibit complex geometries and these geometrical complexities introduce heterogeneities in the stress distribution when the fault slips. The normal and shear stress perturbations introduced are in many cases comparable to the prevailing stresses.

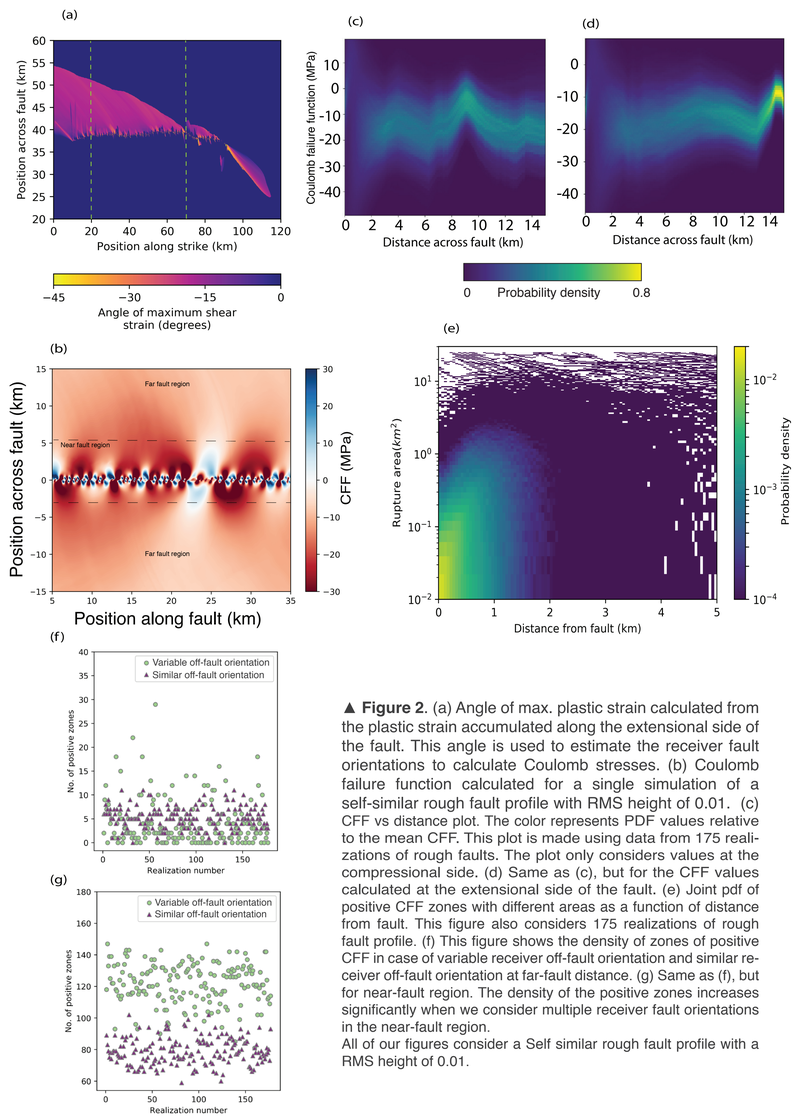

▲ **Figure 2**. (a) Angle of max. plastic strain calculated from the plastic strain accumulated along the extensional side of the fault. This angle is used to estimate the receiver fault orientations to calculate Coulomb stresses. (b) Coulomb failure function calculated for a single simulation of a self-similar rough fault profile with RMS height of 0.01. (c) CFF vs distance plot. The color represents PDF values relative to the mean CFF. This plot is made using data from 175 realizations of rough faults. The plot only considers values at the compressional side. (d) Same as (c), but for the CFF values calculated at the extensional side of the fault. (e) Joint pdf of positive CFF zones with different areas as a function of distance from fault. This figure also considers 175 realizations of rough fault profile. (f) This figure shows the density of zones of positive CFF in case of variable receiver off-fault orientation and similar receiver off-fault orientation at far-fault distance. (g) Same as (f), but for near-fault region. The density of the positive zones increases significantly when we consider multiple receiver fault orientations in the near-fault region.
All of our figures consider a Self similar rough fault profile with a RMS height of 0.01.

Methodology

We couple short-term (i.e. the co-seismic) and long-term (i.e. the inter-seismic) phase of an earthquake, in order to investigate how the induced static stress changes due to rupture on a complex fault influence the dynamics of strain accumulation during inter-seismic phase.

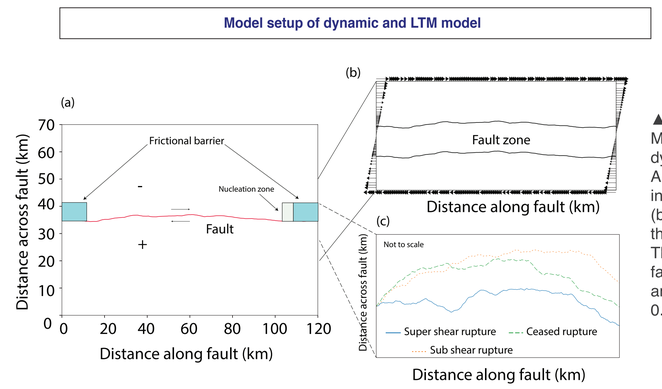

▲ **Figure 3**. (a) Model Setup of our dynamic simulations. A strike slip fault with inherent roughness. (b) Domain setup of the LTM model. (c) Three realization of fault profile with H = 1 and RMS height = 0.01.

We model the off-fault material damage rate dependence using strain softening while the state dependence (i.e. frictional healing) is modeled using state evolution law.

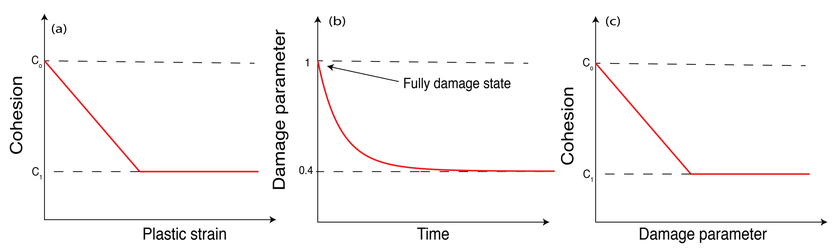

▲ **Figure 4**. (a) Rate dependence is modeled using strain softening. (b) A damage parameter is used to model the state evolution. As the time increases, the damage recovers from its initial state to a healed state. (c) As the damage recovers, the cohesion also recovers. figure (a) and (c) also applies to frictional coefficient.

Results

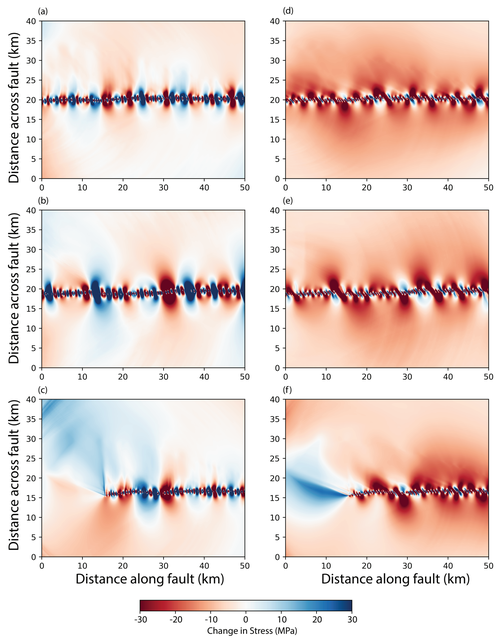

▲ **Figure 5**. Change in stresses at the central part of the domain (taken from 30 to 80 km along fault and 5 to 35 km across fault distance). Figure (a), (b) and (c) are showing change in normal stresses in the central part of modeling domain while (d), (e) and (f) are showing change in shear stresses in the central part of modeling domain. (a) and (d) are figures of sub-shear case. (b) and (e) are figures of super-shear case. (c) and (f) are figures of arrested rupture case.

More Results

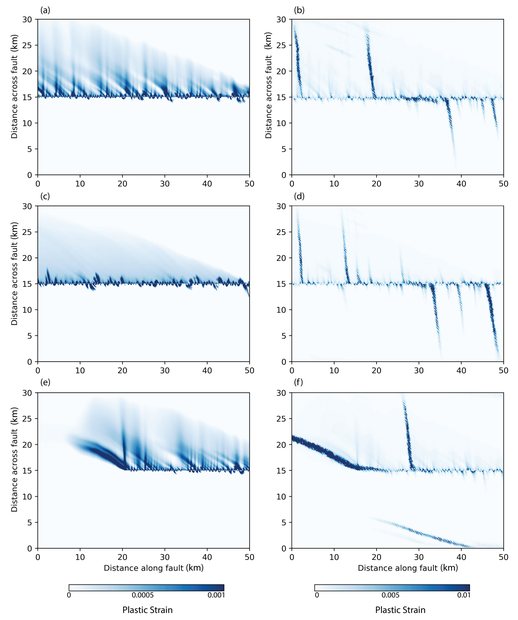

▲ **Figure 6**. Accumulated plastic strain (second invariant of plastic strain tensor) at the central part of the domain. Figures (a) and (b) are for the case of subshear rupture. Figures (c) and (d) are for the case of supershear rupture. Figures (e) and (f) are for the case of arrested rupture. Figures (a), (c) and (e) are showing plastic strain accumulation at time 48 sec for domain 20 to 70 km along fault distance and 15 to 45 across fault distance. Figure (b), (d) and (f) are showing plastic strain accumulated after 200 years for domain 30 to 80 km along fault distance and 15 to 45 across fault distance.

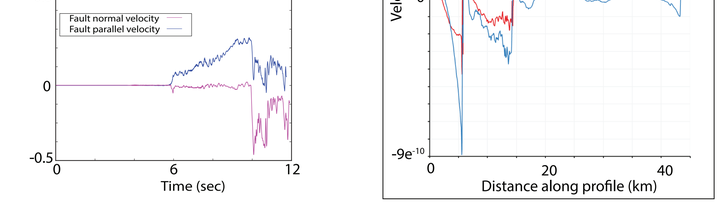

▲ **Figure 7**. (a) Slip rate on the fault as the rupture propagates along the fault in the case of a sub-shear rupture. (b) Velocity at a station 15 km away from the fault profile. (c) Velocity after 44 years of earthquake (during interseismic phase) along a profile parallel to the overall orientation of the fault, but at a distance 5 km away from the fault. The LTM model starts with initial conditions from sub-shear rupture. The boundary is driven with a far-field velocity of $1e^{-9}$ m/sec. (a) and (b) are result of dynamic model, while (c) is taken from the LTM model.

Depth dependent deformation model

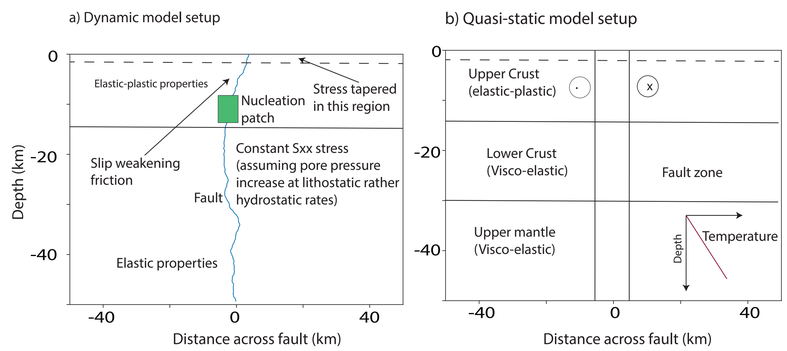

▲ **Figure 8**. (a) The dynamic model setup for the future set of simulations. (b) The quasi-static model setup. (b) Inset shows the temperature profile that will be used for the quasi-static modeling. The viscosity for the lower crust and upper mantle is selected based on the material quartz-diorite and wet olivine respectively.

Acknowledgments

This research was supported by the Southern California Earthquake Center (Contribution No. 8864). We are grateful to the University of Memphis High Performance Computing Center for providing computing facilities to run our simulations.